

**CIRCULATION COPY**  
**SUBJECT TO RECALL**  
**IN TWO WEEKS**

UCRL- 93600  
PREPRINT

**VIBRATION DAMPING IN  
EXTERNALLY PRESSURIZED GAS BEARINGS**

**J. W. Roblee**  
**Lawrence Livermore National Laboratory**

**C. D. Mote, Jr.**  
**University of California**

**This paper was prepared for submittal to the  
International Conference on  
Vibration Problems in Engineering  
Xi'an, China  
June 17-20, 1986**

**June, 1986**

**Lawrence  
Livermore  
National  
Laboratory**

**This is a preprint of a paper intended for publication in a journal or proceedings. Since changes may be made before publication, this preprint is made available with the understanding that it will not be cited or reproduced without the permission of the author.**

**CIRCULATION COPY**  
**SUBJECT TO RECALL**  
**IN TWO WEEKS**

8900

#### DISCLAIMER

This document was prepared as an account of work sponsored by an agency of the United States Government. Neither the United States Government nor the University of California nor any of their employees, makes any warranty, express or implied, or assumes any legal liability or responsibility for the accuracy, completeness, or usefulness of any information, apparatus, product, or process disclosed, or represents that its use would not infringe privately owned rights. Reference herein to any specific commercial products, process, or service by trade name, trademark, manufacturer, or otherwise, does not necessarily constitute or imply its endorsement, recommendation, or favoring by the United States Government or the University of California. The views and opinions of authors expressed herein do not necessarily state or reflect those of the United States Government or the University of California, and shall not be used for advertising or product endorsement purposes.

# VIBRATION DAMPING IN EXTERNALLY PRESSURIZED GAS BEARINGS

Roblee, J. W.\*, and Mote, Jr., C. D.\*\*

## Abstract

The damping mechanisms in externally-pressurized gas bearings are investigated. A single-pole, single-zero transfer function is used to describe the dynamic stiffness of these bearings. The benefits of tuning their frequency-dependent damping are discussed and demonstrated experimentally. A type of auxiliary compensation is also shown to alter the dynamic stiffness of these bearings.

## Introduction

In many machines, the bearings are the largest source of overall compliance. Consequently, the dissipation of energy through damping in the bearing can effectively suppress vibration in the machine. Externally pressurized (EP) gas bearings, commonly used in machines, exhibit damping only over a narrow frequency band. As a result, gas bearings are reputed to be poorly damped in transverse oscillation and are often unstable. The damping mechanisms in flat thrust bearings are examined in this paper. It is shown that EP gas bearings can exhibit significant damping when properly designed.

A common, EP thrust-bearing design is illustrated in Fig. 1, and Fig. 2 shows a pneumatic equivalent of a linearized, lumped-parameter model of the bearing. This is a commonly used dynamic model for EP gas bearings. The gas flows from a constant-pressure supply reservoir at a pressure  $P_s$  through a flow restrictor, typically an orifice, into the bearing recess at a uniform pressure  $P_r$ . The gas leaves the bearing through a gap of uniform thickness  $H$ . This perimeter-region gap acts as a second flow restrictor, which is proportional to  $H^3$ . The area of the piston in Fig. 2 is the effective area  $A_e$  of the bearing, defined as the static bearing load divided by the recess pressure above ambient,  $W/(P_r - P_a)$ . Therefore, the  $A_e$  of Fig. 1 is increased as the area of the recess increases. The recess pressure is determined by enforcing continuity of the mass flow through the gap with the flow through the orifice restrictor. As the gap increases, the equilibrium flowrate increases and the recess pressure decreases, reducing the load  $W$ . This mechanism of flow through two restrictors provides the bearing with its static stiffness  $K_s$ .

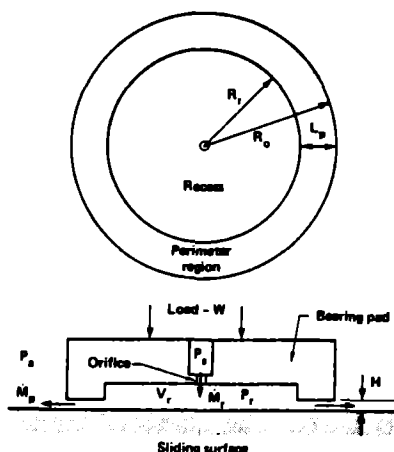


Fig. 1. Geometry of a Typical Externally-Pressurized Gas Bearing.

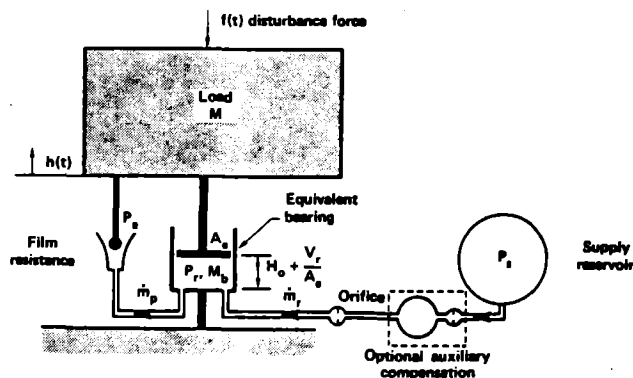


Fig. 2. Pneumatic Equivalent to a Lumped-Parameter EP Gas Bearing Model.

\* Lawrence Livermore National Laboratory, Livermore, California, USA.

\*\* University of California, Berkeley, California, USA.

At very high frequencies of gap fluctuation, the gas becomes trapped in the bearing by its viscosity. The high-frequency stiffness  $K_{\infty}$  of this gas spring is modeled in Fig. 2 by blocking the inlet and outlet of the cylinder,  $\dot{m}_r = \dot{m}_p = 0$ . Note that  $K_{\infty}$  is independent of the active source flow and is therefore passive, whereas  $K_s$  depends upon the source flow and the size of the flow restrictors.  $K_{\infty}$  is increased by decreasing the trapped gas volume. For this reason, gas-bearing designs often use grooves to distribute the gas instead of a recess as shown in Fig. 1. Application of grooves can produce the same pressure distribution and effective area, but with a smaller recess volume  $V_r$  and a larger  $K_{\infty}$ .

#### Damping Mechanisms in EP Gas Bearings

The lumped-parameter model of an EP gas bearing has a dynamic stiffness  $K_b(s)$  that is represented by the equations:

$$K_b(s) = K_s \frac{(1 + \tau_1 s)}{(1 + \tau_2 s)} \quad \text{where} \quad K_{\infty} = \frac{\tau_1}{\tau_2} K_s \quad (1)$$

with  $\tau_1 > 0$ ,  $\tau_2 > 0$ , and the Laplace variable represented by  $s$ . The positive phase shift in dynamic stiffness, between the frequencies  $1/\tau_1$  and  $1/\tau_2$ , results in band-limited damping. The larger the frequency band, the lower the static stiffness  $K_s$  and the higher the damping for a constant  $K_{\infty}$ . (See Curves A and B in Fig. 3.) The damping results from the viscous dissipation in the bearing film and the pressure drop across the orifice. In this respect, the bearing is analogous to a shock absorber with its piston and flow restrictor (Fig. 2). The frequency band of damping narrows as  $K_s \rightarrow K_{\infty}$ . Therefore, the bearing design must be carefully tuned to exploit the damping.

If the active stiffness  $K_s$  exceeds the trapped-gas passive stiffness  $K_{\infty}$ , as shown by Curve C of Fig. 3, the damping is negative and the bearing is unstable. This is illustrated by the transfer function of the pneumatic model in Fig. 2:

$$\frac{h(s)}{r(s)} = \frac{1}{Ms^2 + K_b(s)} \quad (2)$$

Because the phase shift from  $Ms^2$  is  $-180^\circ$ , a negative phase shift at the natural frequency from  $K_b(s)$  results in instability. This instability occurs when the recess pressure variation is out-of-phase with the variation in gap thickness. Consequently, the energy stored in the gas is released out-of-phase with the motion, forcing larger motions.

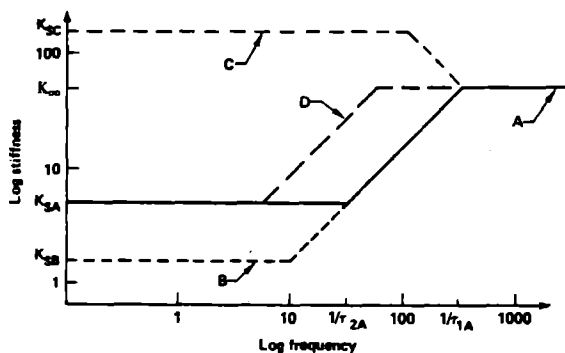


Fig. 3. Amplitude Plot of the Bearing Dynamic Stiffness.

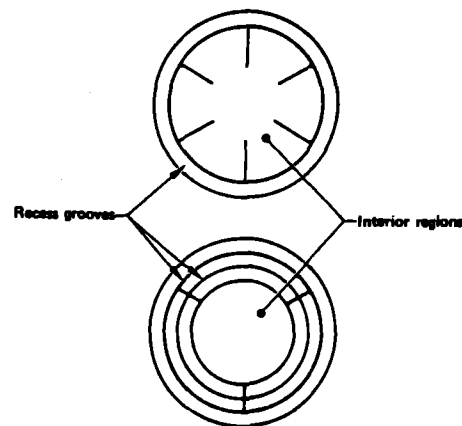


Fig. 4. Possible Recess Groove Layouts.

Many bearing films cannot be modeled with a lumped-parameter analysis. For example, the pressure in regions away from the recess grooves in Fig. 4 will not follow a rapidly changing recess pressure. In addition, if the gap changes rapidly, the gas away from the grooves is

trapped by viscous resistance, which produces a large transient pressure that is independent of the recess pressure. The lumped-parameter model cannot account for this time-dependent, distributed-parameter behavior of the film because it assumes the dynamic pressure distribution is quasi-static.

The interior region can be modeled in part as a squeeze film. A gaseous squeeze film exists when two surfaces, separated only by a thin gas film, are in relative normal motion. The squeeze-film force is determined by integration of the time-dependent pressure distribution generated by the relative motion. The corresponding flowrate into and out of the film is determined by the pressure gradient at the boundary. Both the load and flowrate of a squeeze film with a time-varying boundary pressure are required to model EP gas bearings.

The isothermal Reynold's equation is applicable to squeeze films, as discussed by Langlois.<sup>2</sup> For the small motions of interest here, the Reynold's equation is linearized about the equilibrium point. For a circular disk, the linearized equation is solved in closed form.<sup>2</sup> For a constant boundary pressure of  $1090 \text{ N/m}^2$ , the frequency-dependent, dynamic stiffness of an air squeeze film, 10 cm in diameter and  $8.85 \text{ }\mu\text{m}$  thick, is shown in Fig. 5. Note that the squeeze film behaves as a viscous damper at low frequencies, similar to an incompressible squeeze film, but as a simple spring at high frequencies. As the frequency of gap variation increases, the gas at the center of the bearing film compresses, not being able to flow to the boundary. The radius of this spring-like region of compressing gas grows with frequency until it equals the film radius. This dynamic stiffness is nonlinear in frequency, but it can be linearly approximated by the single pole and single zero shown in Fig. 5. The boundary flowrate and the squeeze-film force, with a time-varying boundary pressure, can also be stated in terms of this linear approximation. This approximate squeeze-film model can then be combined with a lumped-parameter model of the perimeter region to form a hybrid, linear model of bearing dynamics. The squeeze-film forces increase viscous damping at low frequency, but damping at high frequency decreases. Therefore, the frequency band of damping is not increased by a distributed-parameter model, but the band shifts to lower frequencies than those predicted by a simple lumped-parameter model. The dynamic stiffness is represented by (1), with the stiffness of curve D in Fig. 3, instead of Curve A.

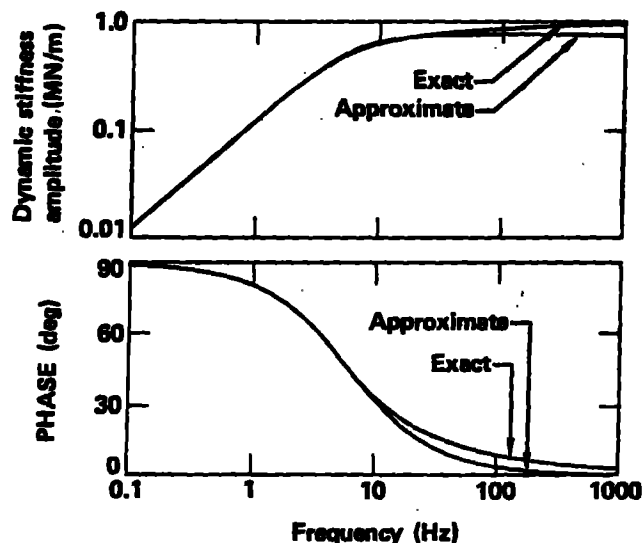


Fig. 5. Dynamic Stiffness of a Circular Squeeze Film (with Air, Boundary Pressure =  $1090 \text{ N/m}^2$ , Gap =  $8.55 \text{ }\mu\text{m}$ , and Diameter = 10 cm).

#### Tuning the Dynamic Stiffness

The high-frequency stiffness  $K_s$  is the primary constraint on the dynamic stiffness of the bearing because it is limited by the gap thickness, supply pressure, bearing area, and load. Therefore, only two free parameters can be tuned. To illustrate a tuned bearing design, the single-degree-of-freedom transfer function (2) is nondimensionalized by substituting (1) and the following parameters:

$$\bar{\alpha} \triangleq \frac{\tau_1}{\tau_2}, \quad \bar{s} \triangleq \tau s, \quad \bar{\kappa} \triangleq \frac{K_{\tau_1}^2}{M}, \quad K_{\tau_2} = \bar{\alpha} K_{\tau_1} \quad (3)$$

giving

$$K_{\tau_2} \frac{-h(\bar{s})}{f(\bar{s})} = \frac{\bar{\kappa} (\bar{\alpha} + \bar{s})}{\bar{s}^2 (\bar{\alpha} + \bar{s}) + \bar{\kappa} (1 + \bar{s})} \quad (4)$$

The transfer function is characterized by  $\bar{\alpha}$  and  $\bar{\kappa}$ . Note that  $\bar{\kappa}^{1/2}$  is the dimensionless natural frequency of the mass  $M$  on the spring  $K_{\tau_2}$ . The real pole and zero of (4) occur above the resonant frequency, and nearly cancel for  $\bar{\kappa} < 4$ . Therefore, they have little effect on the transfer function. One of the complex conjugate poles ( $\bar{\lambda}_r$  and  $\bar{\lambda}_i$ ) are plotted in Fig. 6 for different  $\bar{\alpha}$  and  $\bar{\kappa}$ . The complex root loci are plotted for constant  $\bar{\alpha}$  in Fig. 6a and for constant  $\bar{\kappa}$  in Fig. 6b. The tick marks on the plotted loci denote intersections with those of the other figure, and indicate the parameter sensitivity of the complex pole. In Fig. 6a, as  $\bar{\alpha} \rightarrow 1$ ,  $\bar{\lambda}_r \rightarrow 1$ ; meaning that damping decreases and the roots approach the imaginary axis. For  $\bar{\alpha} < 1$ , the loci would be in the right half plane,  $\bar{\lambda}_r > 0$ , indicating an instability. For large  $\bar{\kappa}$ ,  $\bar{\lambda}_r$  is asymptotic to  $(1-\bar{\alpha})/2$  and  $\bar{\lambda}_i = \bar{\kappa}^{1/2}$ . Note that  $\bar{\lambda}_r$  and  $\bar{\lambda}_i \rightarrow 0$  as  $\bar{\kappa} \rightarrow 0$ , meaning that the model becomes ideally inertial as the bearing stiffness vanishes. When  $\bar{\alpha} = 1$ ,  $\bar{\lambda}_r = 0$  and  $\bar{\lambda}_i = \bar{\kappa}^{1/2}$ , indicating that damping is nonexistent. As  $\bar{\alpha}$  increases, the static stiffness  $K_{\tau_2}$  decreases when  $\bar{\kappa}$  is constant, forcing the pole towards the origin in Fig. 6b. For each  $\bar{\alpha} = \text{constant}$  locus a unique  $\bar{\kappa}$  corresponds to the maximum damping ratio. This is a reasonable design goal. Once the desired  $\bar{\alpha}$  and  $\bar{\kappa}$  are determined from Fig. 6, they can be related to a particular bearing design.

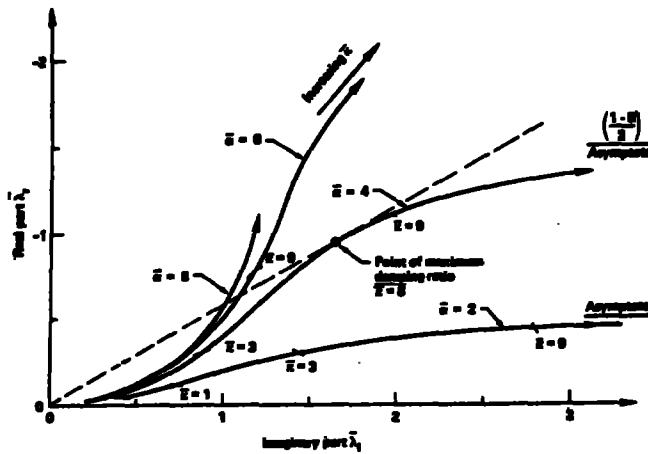


Fig. 6a. Root Loci of (4) for  $\bar{\alpha} = 2, 3, 6, 8$ .

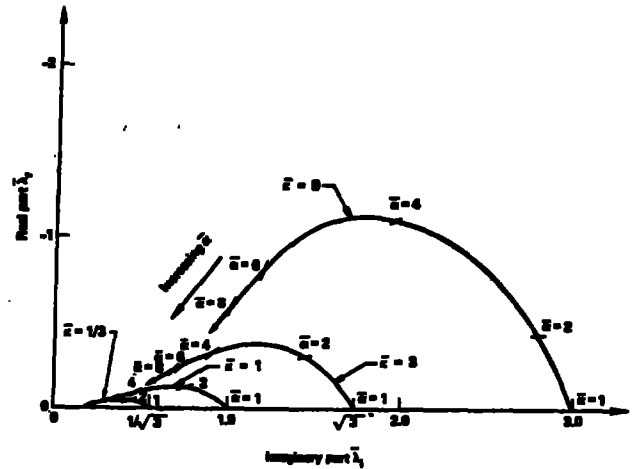


Fig. 6b. Root Loci of (4) for  $\bar{\kappa} = 1/3, 1, 3, 9$ .

#### Auxiliary Compensation

An alternative bearing compensation technique, one that is easily tuned, uses an additional chamber and restrictor in the supply line (Fig. 2). This chamber decouples the two flow restrictors at high frequencies. For low-frequency pressure fluctuations, the decoupling effect of the chamber volume is small, and the two supply-line restrictors behave as one. Typically, the pressure drop across the upstream restrictor is much larger than that across the downstream restrictor. At higher frequencies, downstream pressure variations are not transmitted upstream by the chamber, effectively making it a constant-pressure reservoir. For this reason, the upstream supply-line restrictor does not affect the high-frequency bearing response, which allows the static stiffness to be tuned independent of the high-frequency stiffness. An otherwise unstable bearing can be stabilized in this manner. For example, consider the dynamic stiffness plotted in Fig. 7, which has an extra pole and an extra zero at low frequencies, which result from using auxiliary compensation. This bearing design would normally be unstable because  $K_{\tau_2} > K_{\tau_1}$ . However, the phase shift at high frequency is positive as a result of the additional chamber and restrictor, and the bearing is therefore stable for high frequency resonances.

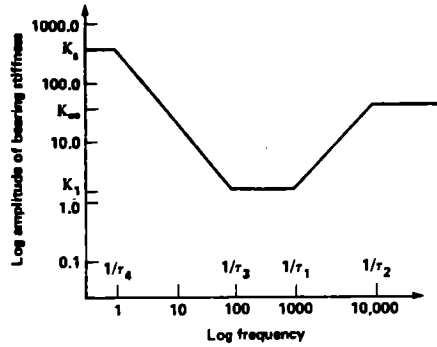


Fig. 7. Amplitude Plot of the Dynamic Stiffness of a Bearing with Auxiliary Compensation.

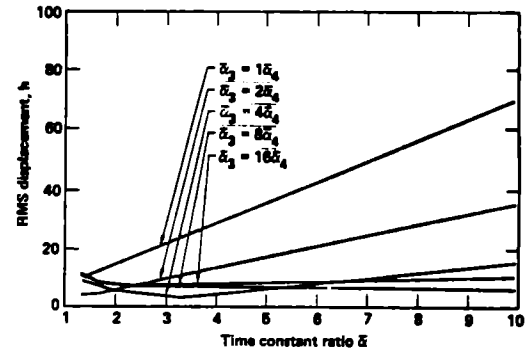


Fig. 8. Root Mean Square Displacement of (2) and (5) for a Band-Limited White Noise Disturbance Force.

The dynamic stiffness of a bearing with this type of auxiliary compensation is:

$$\bar{K}_b(\bar{s}) \triangleq \frac{K_b(\bar{s})}{K_\infty} = \frac{(1+\bar{s})(\bar{\alpha}_3+\bar{s})}{(\bar{\alpha}+\bar{s})(\bar{\alpha}_4+\bar{s})} ; \bar{\alpha}_3 \triangleq \frac{\tau_1}{\tau_3} ; \bar{\alpha}_4 \triangleq \frac{\tau_1}{\tau_4} ; K_\infty = \frac{\bar{\alpha} \bar{\alpha}_4}{\bar{\alpha}_3} K_s \quad (5)$$

Assuming that  $K_\infty$ ,  $\tau_1$ , and  $\tau_2$  are determined by tuning the downstream restrictor,  $\tau_3$  and  $\tau_4$  are tuned to increase bearing stiffness at low frequency. However, a condition where  $\tau_3 \gg \tau_1$  is required so that the high-frequency damping is not significantly reduced. In addition, the natural frequencies must be greater than  $1/\sqrt{\tau_3\tau_1}$  to avoid a negative phase shift, which would result in instability. To illustrate the benefit of the additional chamber and restrictor (and of the corresponding low-frequency pole and zero), the root-mean-square response of the mass  $M$  in (2) is calculated for a band-limited white-noise disturbance force,  $f(t)$ . The results are graphed in Fig. 8. Note the large reduction in response for  $\bar{\alpha}_3 > \bar{\alpha}_4$  with respect to the case  $\bar{\alpha}_3 = \bar{\alpha}_4$ , where the auxiliary-compensation terms drop out.

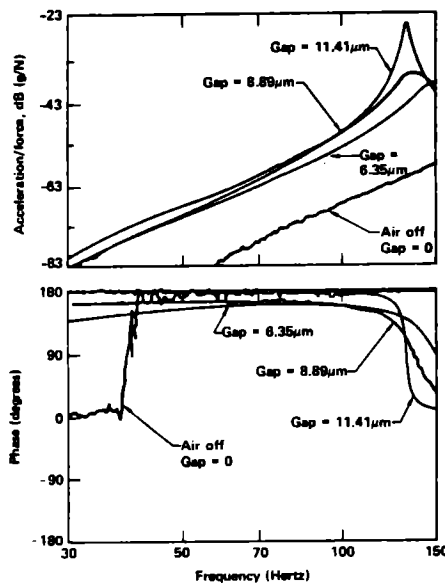


Fig. 9. Acceleration-to-Force Transfer Functions of the Bearing-Slide System for  $W = 222$  N, and Different Gap Thicknesses.

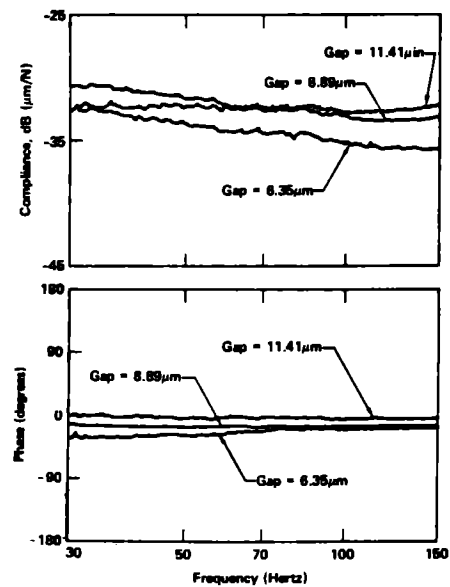


Fig. 10. Dynamic Compliance of the Bearing for  $W = 222$  N, and Different Gap Thicknesses.

## Experimental Results

The experimental apparatus consisted of a translating slide mounted on four parallel reed flexures which allow translation without rotation. A standard 15 x 15 x 10-cm machinist's parallel block and a precision-lapped 15-cm granite cube were mounted within the slide assembly. The granite cube was one bearing surface; the other was a grooved pad, 6.3 cm in diameter and 2.5 cm thick. The bearing pad was mounted on a ball pivot that allowed self-alignment of the pad with respect to the granite cube. The cube was preloaded against the bearing by compressing a soft helical spring. The groove was located on a 5.5 cm diameter on the pad and was 0.25 mm square in cross section. The groove was supplied by air flow from three 0.2mm diameter orifices, spaced 120° apart along the groove. The use of three restrictors allowed the groove to be small, and gave the bearing the ability to right itself on the ball pivot.

A set of acceleration-to-force transfer functions for the bearing-slide system is presented in Fig. 9 for a 222 N preload on the bearing, and for different gap thicknesses (achieved by changing the supply pressure). These curves correspond to the second derivatives of the transfer functions of (2). The resonance near 130 Hz is associated with the translation of the slide assembly on the EP air bearing. Note that the amplitude decreases and damping increases by an order-of-magnitude as the gap is reduced, demonstrating the significance of tuning the dynamic compliance of the bearing. The lightly damped resonance at the 11.41  $\mu\text{m}$  gap shows that the bearing design is near its threshold of instability at that gap. A transfer function measured at a 3.81  $\mu\text{m}$  gap, which is not shown in Fig. 9, had a maximum amplitude that is slightly larger than that at the 6.35  $\mu\text{m}$  gap. This occurs because the frequency band of bearing damping has shifted below the natural frequency. The transfer functions in Fig. 9, the mass of the slide, and (2) are used to predict the dynamic compliance of the bearing,  $1/K_b(s)$ , in Fig. 10. The trend towards smaller compliance and increased damping for smaller gaps is observed. The plots in Fig. 10 correspond to the inverse of the stiffness plots in Fig. 3. The limited frequency range of the measurements does not show the high and low frequency trends in the stiffness, as does those plots in Fig. 3. However, these experimental results demonstrate how just one, of the many possible bearing parameters, can be tuned to influence the dynamic stiffness of EP gas bearings.

## Conclusions

Damping mechanisms in EP gas bearings are the result of time-varying gas flow through restrictors, and from the gas squeeze film. The high-frequency limit to damping results from the compressibility of the gas trapped in the bearing. For single-restrictor grooved bearings, the dynamic stiffness is described by a single pole and zero, which determine the frequency band of the damping. This pole and zero greatly influence the dynamics of the machine-bearing system, including its possible instability. This was experimentally demonstrated by an order-of-magnitude variation in damping at resonance. Therefore, to make use of the available damping in a bearing, it must be tuned for a particular application. A second flow restrictor and a chamber in the supply line add another, independently tunable, pole and zero to the dynamic stiffness of the bearing. This auxiliary compensation makes possible a high static stiffness with damping at high frequency.

## Acknowledgments

The authors would like to thank Patricia Flowers, Linda Sarginson and Stephen Greenberg for their help in the preparation of this manuscript.

## Auspices

Work performed under the auspices of the U.S. Department of Energy by the Lawrence Livermore National Laboratory under Contract No. W-7405-ENG-48.

## References

1. Roblee, J. W., Design of Externally Pressurized Gas Bearings for Dynamic Applications Ph.D. Thesis, University of California, Berkeley, CA, April, 1985. Available through University Microfilms.
2. Langlois, W. E., "Isothermal Squeeze Films," Quarterly of Applied Mathematics, Vol. XX, No. 2, 1962, pp. 131-150.